JACS
JOURNAL OF THE AMERICAN CHEMICAL SOCIETY

ARTICLE

pubs.acs.org/JACS

Synthesis and Charge-Transfer Chemistry of $La_2@I_h$-C_{80}/$Sc_3N@I_h$-C_{80}−Zinc Porphyrin Conjugates: Impact of Endohedral Cluster

Lai Feng,[†] Shankara Gayathri Radhakrishnan,[‡] Naomi Mizorogi,[†] Zdenek Slanina,[†] Hidefumi Nikawa,[†] Takahiro Tsuchiya,[†] Takeshi Akasaka,[*,†] Shigeru Nagase,[*,§] Nazario Martín,[#,∥] and Dirk M. Guldi[*,‡]

[†]Center for Tsukuba Advanced Research Alliance, University of Tsukuba, Tsukuba 305-8577, Japan

[‡]Department of Chemistry and Pharmacy & Interdisciplinary Center for Molecular Materials, Friedrich-Alexander-Universität Erlangen-Nürnberg, 91058 Erlangen, Germany

[§]Department of Theoretical and Computational Molecular Science, Institute for Molecular Science, Okazaki 444-8585, Japan

[#]Departamento de Química Orgánica, Facultad de Química, Universidad Complutense, 28040 Madrid, Spain

[∥]IMDEA-Nanoscience, Campus de Cantoblanco, 28049 Madrid, Spain

Supporting Information

ABSTRACT: Two stable electron donor−acceptor conjugates, that is, **3** and **5b**, employing $La_2@I_h$-C_{80} and $Sc_3N@I_h$-C_{80}, on one hand, and zinc tetraphenylporphyrin, on the other hand, have been prepared via [1 + 2] cycloaddition reactions of a diazo precursor. Combined studies of crystallography and NMR suggest a common (6,6)-open addition pattern of **3** and **5b**. Still, subtly different conformations, that is, a restricted and a comparatively more flexible topography, emerge for **3** and **5b**, respectively. In line with this aforementioned difference are the electrochemical assays, which imply appreciably stronger I_h-C_{80}/ZnP interactions in **3** when compared to those in **5b**. Density functional calculations reveal significant attractions between the two entities of these conjugates, as well as their separately localized HOMOs and LUMOs. The geometrical conformations and LUMO distributions of **3** and **5b**, at our applied computational level, are slightly varied with their different endohedral clusters. The clusters also exert different impact on the excited state reactivity of the conjugates. For example, **3** undergoes, upon photoexcitation, a fast charge separation process and yields a radical ion pair, whose nature, namely, $(La_2@C_{80})^{\bullet-}-(ZnP)^{\bullet+}$) versus $(La_2@C_{80})^{\bullet+}-(ZnP)^{\bullet-}$), varies with solvent polarity. **5b**, on the other hand, afforded the same $(Sc_3N@C_{80})^{\bullet-}-(ZnP)^{\bullet+}$) radical ion pair regardless of the solvent.

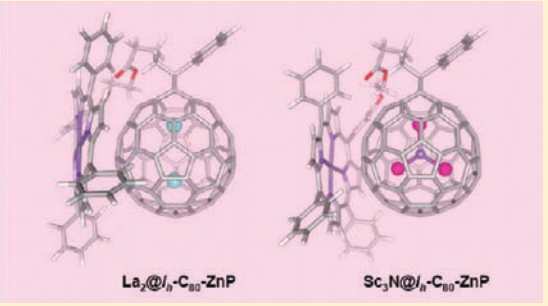

INTRODUCTION

The ineluctable and continuing depletion of fossil fuels poses one of the greatest challenges to mankind. Sunlight with its interminable radiation has been the source for all of the photosynthetic organisms, where energy storage is realized via chemical bond formation.[1] Thus, photosynthesis, which has emerged as a blue print for solar energy storage, has motivated the application of "photosynthesis" fundamentals in the design of artificial reaction centers.[2]

Excitonic binding energies in organic donor−acceptor conjugates, which range from 0.2 to 1.0 eV, ensure an efficient charge splitting and charge transport as a means to create appreciable photocurrent.[3] The advent of molecular conductors began in 1973 with the demonstration of charge transfer/charge transport in an organic metal, tetrathiafulvalene (TTF).[4] In the following years, breakthroughs such as the introduction of interfacing two organic semiconductors, that is, an electron donor and an electron acceptor, paved the road to organic solar cells.[5] The latter created a boom in the field of electron donor−acceptor systems as a means to generate spatially and electronically well-isolated radical ion pairs.

Empty fullerenes, in general, and C_{60}, in particular, exhibit all of the hallmarks that are found in nature's most sophisticated and important solar energy conversion/storage system, namely, photosynthetic organisms in plants, algae, and a variety of types of bacteria. Owing to its rigid structure, C_{60} possesses small reorganization energies in charge transfer reactions, which is of particular interest and, which, as a matter of fact, has exerted noteworthy impact on the improvement of charge separation processes triggered by light.[6]

Empty fullerenes are capable of hosting metal atoms in their interior and, thereby, forming endohedral metallofullerenes (EMF). EMFs possess impressive electronic structures that are governed by significant electron transfer between the encapsulated species and the fullerene.[7,8] To this end, control over the encapsulated species results in a large variety of EMFs that feature distinct chemical and physical properties.[7]

$La_2@I_h$-C_{80} and $Sc_3N@I_h$-C_{80} are two well-studied EMFs with close-shell structure.[9−11] They possess the same I_h-C_{80} cage

Received: March 15, 2011
Published: April 21, 2011

dx.doi.org/10.1021/ja202331r | J. Am. Chem. Soc. 2011, 133, 7608–7618

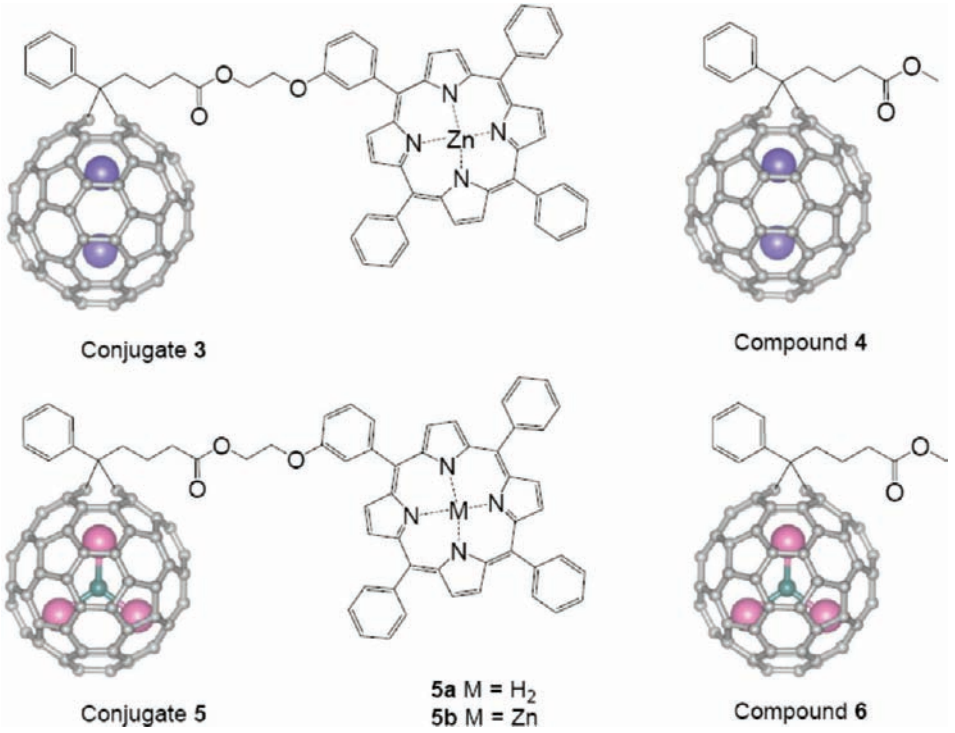

Figure 1. Schematic structures of the described and investigated compounds.

and similar electronic structures, which are usually described as $(La_2)^{6+}@I_h\text{-}C_{80}{}^{6-}$ and $(Sc_3N)^{6+}@I_h\text{-}C_{80}{}^{6-}$. Owing, however, to the different type of endohedral guests (i.e., $(La_2)^{6+}$ versus $(Sc_3N)^{6+}$), their chemical reactivity and electrochemical property differ. In particular, the first reduction potential of $La_2@I_h\text{-}C_{80}$ is much higher than that of $Sc_3N@I_h\text{-}C_{80}$, which reflects the impact on the LUMO level. Moreover, comparing the on-set potential gap of $La_2@I_h\text{-}C_{80}$ (0.87 eV) with those of $Sc_3N@I_h\text{-}C_{80}$ (1.86 eV), and C_{60} (2.33 eV),[11a,12] the small band gap of $La_2@I_h\text{-}C_{80}$ is impressive and even comparable with those of a few conducting polymers, whose electrochemical or optical gaps are smaller than 1.0 eV.[13] $Sc_3N@I_h\text{-}C_{80}$, on the other hand, attracts attentions due to the higher LUMO level and the unique electronic structure. All these features allow them and their analogues to be exploited in molecular electronics and electron donor−acceptor systems.[14−16]

Coupling redox and/or photoactive building blocks to fullerenes,[17] especially to C_{60}, has resulted in electron donor−acceptor conjugates with band gaps of 1−2 eV.[18] We have recently reported on $Sc_3N@I_h\text{-}C_{80}$ and $La_2@I_h\text{-}C_{80}$ based electron donor−acceptor conjugates using ferrocene, triphenyl amine, and π-extended TTF donors.[15] Duality in the electron/hole accepting nature was also recently reported for a $Ce_2@C_{80}$ based conjugate, but $Ce_2@C_{80}$ features, in contrast to $La_2@C_{80}$, two unpaired electrons for each incorporated Ce.[16]

Porphyrins, the synthetic analogues of chlorophyll, have been extensively used as electron donating chromophores.[19] Furthermore, porphyrins give rise to remarkable interactions with EMFs owing to their large $\pi-\pi$ surface.[20]

In the present work, two EMFs, namely, $La_2@I_h\text{-}C_{80}$ and $Sc_3N@I_h\text{-}C_{80}$, are conjugated to zinc tetraphenylporphyrin (ZnP) via [1 + 2] cycloaddition yielding novel $La_2@I_h\text{-}C_{80}$−ZnP (**3**) and $Sc_3N@I_h\text{-}C_{80}$−ZnP (**5b**), respectively, see Figure 1. Our synthetic efforts have enabled for the very first time a systematic comparison between two stable and isoelectronic endohedral metallofullerenes. Any differences in terms of, for example, physicochemical features, including electron transfer chemistry, should unambiguously evolve from the endohedrally entrapped clusters, that is, Sc_3N versus La_2. In fact, a thorough investigation documents that indeed the entrapped cluster has a significant impact on the electron transfer chemistry.

RESULTS AND DISCUSSION

Synthesis and Structural Characterizations. Conjugates **3** and **5** were synthesized using the respective EMFs via the reaction of a diazo precursor (Supporting Information Scheme S1). The reaction was facile in the case of **3** and was stopped when the ratio of the conjugate to pristine $La_2@I_h\text{-}C_{80}$ exceeded 2:1. The synthesis of **5b** was done in two steps, namely, the synthesis of $Sc_3N@I_h\text{-}C_{80}$−H_2P (**5a**) followed by the insertion of zinc (Scheme S2). Notable is that the first step took nearly 20 h in spite of the similar scale and reaction conditions as used for **3**. This implies a higher reactivity of $La_2@I_h\text{-}C_{80}$ toward diazo-compound when compared to that of $Sc_3N@I_h\text{-}C_{80}$. As references, compounds **4** and **6** were synthesized. All of the compounds were separated and purified using high-performance liquid chromatography (HPLC). Their molecular integrities were confirmed by MALDI-TOF spectrometry, in which only molecular ion peaks were found at 2130.96 m/z for conjugate **3**, 2004.04 m/z for conjugate **5b**, and 1427.90 m/z for compound **4** (Figure S3). Absence of other fragment peaks in the spectra of these [1 + 2]-adducts confirmed their robust structures and high stabilities under laser decomposition conditions. The samples are very stable and could be stored in the dark under Ar without showing any decomposition within 6 months.

Figure 2 shows the X-ray structure of **4** and confirms the (6,6)-open addition pattern[21] as reported previously for $Ce_2@I_h\text{-}C_{80}$

dx.doi.org/10.1021/ja202331r |J. Am. Chem. Soc. 2011, 133, 7608–7618

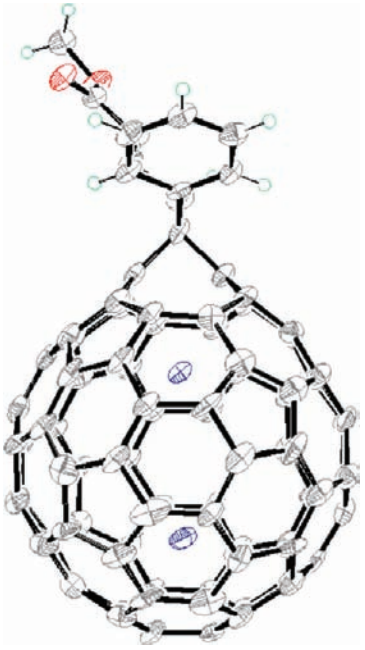

Figure 2. ORTEP drawing of **4** (major enantiomer). The CS_2 molecules are omitted for clarity.

and $Sc_3N@C_{80}$ analogues (**2** and **6**).[16,22] Thus, the metallofullerenes of **2**, **4**, and **6** likely retain a 86 π-electron configuration, that is, 80 π-electrons from C_{80} and six electrons from the encapsulated cluster. The La_2 cluster is highly localized and collinear with the spiro C atom, which is in line with the structure of **2**. The distance between the two La atoms is 4.030 Å, slightly shorter than the Ce···Ce distance (4.059 Å) in **2**.[16] On the other hand, although I_h-C_{80} cage of **4** reveals disorder due to the presence of a pair of enantiomers, La_2 cluster has no disorder, reflecting its highly localized position. In contrast, the X-ray structure of **6**[22] shows a highly localized Sc atom that has an orientation pointing toward the spiro C atom, while the other two Sc atoms are more delocalized and present a couple of disorders, indicating the 2D-rotation of the Sc_3N cluster. This subtle difference between the endohedral structures of **4** and **6** might facilitate the understanding of the differences between **3**/**4** and **5**/**6** obtained from the NMR experiments.

NMR experiments were performed to investigate the structures of **3** and **5**, which failed to form single crystals (Figure 3). Initially, we focused on **3** and **4** owing to their structural similarity. Chemical shifts of the two substituted carbons of $La_2@C_{80}$ in the ^{13}C NMR spectra are observed at δ = 107.00/93.29 ppm for **4** and δ = 106.56/93.00 ppm for **3**, indicating a similar addition pattern as well as the alignment of the La_2 cluster. Two pairs of broad signals in the ^1H NMR spectra of **4**, centered at δ = 3.46/3.56 ppm and 2.49/2.61 ppm, are assigned to the geminal protons of two methylene groups adjacent to I_h-C_{80} and were corroborated by H−H COSY experiments (Figure S4). In contrast, methylene groups that are farther away from C_{80}-I_h gave rise to a triplet signal at δ = 2.66 ppm. The lack of difference between its two geminal protons suggests that only the geminal protons of the methylene groups adjacent to I_h-C_{80} are present in subtly different chemical environments. On the other hand, the phenyl group of **4** gave rise to five ^1H signals in the field of 7.5−9 ppm. With the help of COSY experiments all of the latter were assigned to the phenyl group. Differences of $\Delta\delta$ = 0.55 and 0.06 ppm for the two *ortho*- and *meta*-protons, respectively, confirm that the phenyl carbons were magnetically nonequivalent. This trend was further corroborated by DEPT135 and HMQC experiments (Figures S6 and S7). Herein, implicit is the hindered rotation of phenyl group caused by the $La_2@I_h$-C_{80} moiety. In fact, the latter is believed to be responsible for perturbations that are comparable to those seen for $Ce_2@C_{80}$ analogue.[16]

The ^1H NMR spectrum of conjugate **3**, on the other hand, shows upfield shift for the methylene protons ($\Delta\delta$ = 0.29 and 0.21 ppm) due to shielding effects posed by the ZnP moiety. In the lower field, the ^1H signals from the phenyl group and those from phenyl groups of ZnP moiety appeared between 7.2 and 8.6 ppm. Notable is a partial overlap, which imposes difficulties in the assignments. Nevertheless, better resolved are the β-pyrrole proton signals of ZnP in the 8.6−9.0 ppm region. In particular, four of them appeared as separated doublets, while the other four overlapped to afford a triplet (*2H*) and a more intensive doublet (*2H*). Such magnetically nonequivalent β-pyrrole protons are comparable with those of the C_{60}−ZnP conjugates, in which C_{60} and ZnP moieties are closely placed.[23] To this end, we assume a close proximity between the two chromophores as well as a constrained conformation. Considering the flexibility of the spacer, $La_2@C_{80}$ and ZnP might attract each other via unusual strong π stacking and electrostatic interactions.

Next, we turned to conjugate **5** and its reference **6**. The ^{13}C NMR spectrum of **5a** exhibits resonances of two substituted carbons at δ = 95.77/95.10 ppm, which is in close resemblance with those of **6** (δ = 96.49/95.55 ppm). It is notable that these two carbons are chemically different, namely, pyrene-like and corannulene-like carbons, respectively. However, they differ by less than 1 ppm for **5a**/**6** whereas by nearly $\Delta\delta$ = 13 ppm for **3**/**4**. Taking the X-ray analyses into account, it is likely that the more delocalized Sc_3N cluster of **5a**/**6** results in a more isotropic I_h-C_{80} relative to **3**/**4** with their standing La_2 cluster. Interestingly, unlike **4**, the ^1H NMR spectrum of **6** suggests more equivalent *ortho*/*meta*-phenyl protons and methylene protons, the former leading us to hypothesize a more freely rotated phenyl group. On the other hand, the porphyrin protons of **5a** and **5b** give rise to rather broad ^1H signals, reflecting an intramolecular flexibility. Therefore, $La_2@I_h$-C_{80} appears to impose a stronger perturbation on the attached groups than $Sc_3N@I_h$-C_{80}.

Electrochemical Studies. The electrochemical properties of **3**−**6** were investigated by differential pulse voltammetry (DPV) and cyclic voltammetry (CV) in *o*-dichlorobenzene using 0.05 M *n*-Bu_4NPF_6 as supporting electrolyte (Figure 4 and Figure S13−16). The DPV results are summarized in Table 1. **4** gave rise to two oxidation (i.e., 0.49 and 0.89 V) and three reduction processes (i.e., −0.36, −1.76, and −2.19 V). Compared with pristine $La_2@I_h$-C_{80}, the first reduction and the first oxidation of **4** are cathodically shifted by ca. 50 and 70 mV, respectively. **3** reveals four well-resolved oxidation processes at 0.33, 0.52, 0.65, and 0.88 V. The third and fourth oxidations correspond well with the second oxidation of ZnP and the second oxidation of **4**, respectively. Importantly, the first oxidation is 60 mV lower than that of ZnP and the second oxidation is 30 mV higher than the first oxidation of **4**. Considering that the first oxidation of $La_2@C_{80}$ is centered at I_h-C_{80}, an easier ZnP oxidation and a more difficult I_h-C_{80} oxidation prompts to a change in charge transfer chemistry. When turning to the reduction, we note that the first reduction of **3**, which occurs at −0.39 V and which involves the La_2 cluster, is cathodically shifted by 30 mV relative

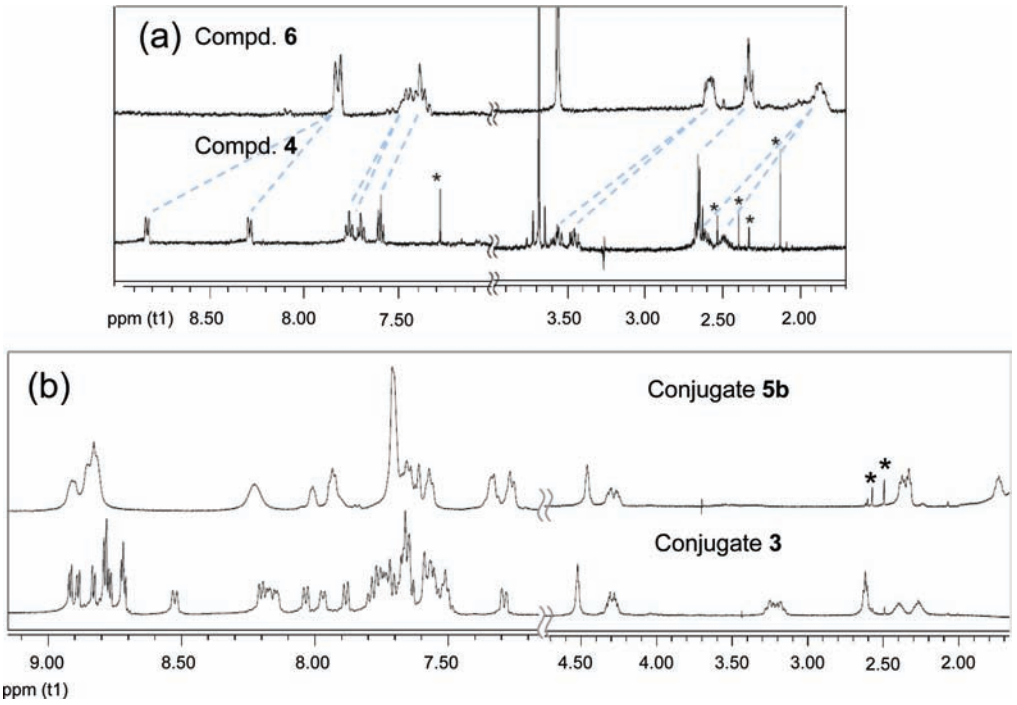

Figure 3. ^{1}H NMR spectrum of (a) **4**/**6** and (b) **3**/**5b** in $C_2D_2Cl_4$. Asterisk (*) refers to the signals that were caused by impurities or solvents. The dashed lines represent the spectral changes due to the different endohedral cluster.

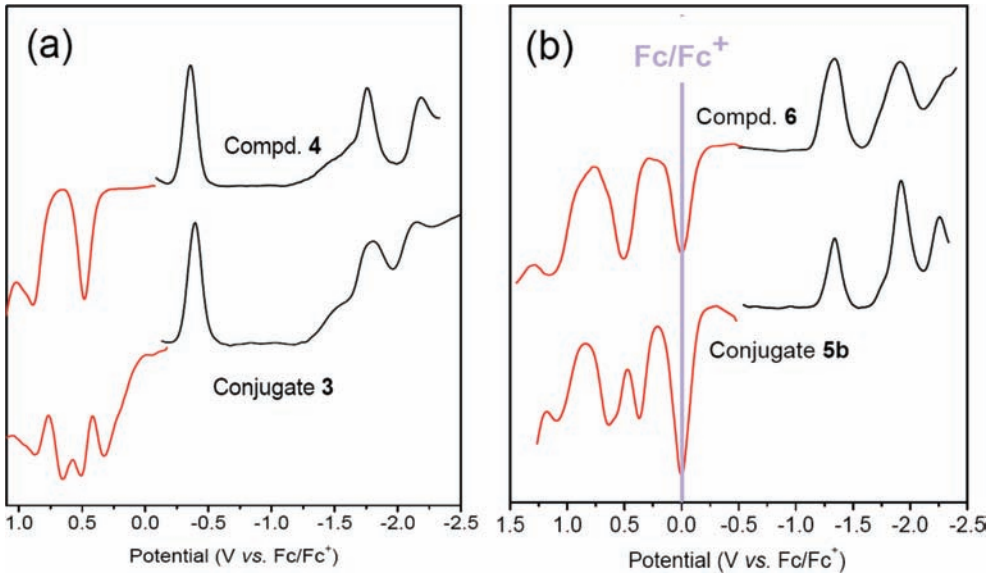

Figure 4. Differential pulse voltammograms of (a) **3** and **4** and (b) **5b** and **6**.

to that of **4**. Owing to the strong mutual $La_2@C_{80}$/ZnP interactions, the reduction is impeded, which was also seen for *trans*-2-C_{60}−ZnP adduct.[24] At more negative potentials, two more reduction processes (i.e., −1.79 and −2.15 V) are observed. Both of the latter involve $La_2@C_{80}$. It should be noted that the ZnP reduction is masked by the $La_2@C_{80}$ reductions. Complementary CV experiments confirmed the reversibility of the first oxidation and the first reduction in **4**, on one hand, and all of the redox processes involving $La_2@C_{80}$ as well as the first oxidation of ZnP in **3**, on the other hand.

5b shows three oxidation and three reduction processes. With regard to **6** and ZnP, the first (i.e., 0.37 V) and the third oxidation (i.e., 1.10 V) of **5b** are assigned to ZnP and $Sc_3N@C_{80}$, respectively. The second oxidation is an overlap of two one-electron oxidation processes, in which, nevertheless, the $Sc_3N@C_{80}$ oxidation is buried by the dominating ZnP oxidation (i.e., 0.64 V). In the cathodic part, the first (i.e., −1.34 V) and third reduction (i.e., −2.26 eV) were assigned with confidence to $Sc_3N@C_{80}$ and ZnP, respectively. On the contrary, the second reduction (i.e., −1.92 V) is an overlap of $Sc_3N@C_{80}$ and ZnP oxidations.

Owing to the conformational flexibility of **5b**, mutual $Sc_3N@C_{80}$/ZnP interactions play, at best, a minor role. As a matter of fact, **6** and **5b** showed almost unaltered first oxidation and reduction potentials. In CV studies, **6** showed irreversible first oxidation and reduction at a scan rate of 100 mV/s, in line with other reported [1 + 2]-adducts of $Sc_3N@C_{80}$.[25] In **5b**, fully reversible was the first oxidation that is based on ZnP.

Theoretical Calculations. To evaluate the intramolecular interactions and the electronic structures of **3** and **5b**, DFT calculations were performed with *Gaussian 09* package.[26] Herein, the new M06-2X functional[27] of Zhao and Truhlar was employed because of its higher reliability in accounting for nonbonding interactions than the customary B3LYP functional.[28] As shown in Figure 5, folded molecular models of **3** and **5b** were separately constructed via the DFT-based optimization process, indicating significant interfragment attractions at the applied computational level. It is notable that in the energy minimum the La_2 cluster is collinearly arrayed with the spiro carbon, whereas the Sc_3N cluster is standing with one Sc-atom pointing to the spiro carbon and another one being adjacent to the ZnP moiety. The center-to-center distances between the two moieties of **3** and **5b** are 6.57 and 6.75 Å, while their shortest Zn-to-cage distances are 2.65 and 2.75 Å, respectively. These results suggest that the alternation of La_2 cluster with Sc_3N cluster induces slightly longer interfragment distance and somewhat different conformation. On the other hand, the calculated HOMOs and LUMOs of conjugates are separately centered on ZnP and metallofullerene entities. For **3**, a delocalization of HOMO on C_{80} cage, to a small extent, is observed, indicating more evident ground-state interaction. The distribution of LUMO is clearly sensitive to the endohedral cluster: for **3**, it is mostly localized on the La_2 cluster, whereas for **5b**, it is only partially on the Sc_3N cluster. Generally, these separately localized HOMOs and LUMOs might suggest the possible formations of charge separated states of **3** and **5b**, that is, $(La_2@C_{80})^{\bullet-}-(ZnP)^{\bullet+}$ and $(Sc_3N@C_{80})^{\bullet-}-(ZnP)^{\bullet+}$. In addition, our theoretical approach ignores solvent effect that may reduce the $\pi-\pi$ interaction to some extent, but it explains those observed experimentally in spectroscopic and electrochemistry studies and, we believe, provides a powerful insight into the origins of those intramolecular interactions in terms of the most simplified model.

Table 1. Redox Potentials of Conjugates 3, 5b and Reference Compounds[a]

	E_{ox4}	E_{ox3}	E_{ox2}	E_{ox1}	E_{red1}	E_{red2}	E_{red3}
$La_2@C_{80}$			0.95	0.56	−0.31	−1.71	−2.13
4			0.89	0.49	−0.36	−1.76	−2.19
3	0.88	0.65	0.52	0.33	−0.39	−1.79[b]	−2.15[b]
ZnP			0.65	0.39	−1.94	−2.27	
5b	1.10	0.64	0.55[c]	0.37	−1.34	−1.92[b]	−2.26
6			1.15	0.52	−1.33	−1.91	
$Sc_3N@C_{80}$			1.09[a]	0.59	−1.27	−1.66	

[a] All the potentials, in volts, were corrected relative to the $Fc^{0/+}$. [b] Two-electron reduction process. [c] Indicates the estimated value.

Photophysical Studies. The absorption spectra of **3**−**6** in toluene solution are summarized in Figure 6. It is evident that the absorption features of **4** and **6** are almost identical with those of pristine $La_2@C_{80}$ and $Sc_3N@C_{80}$, respectively. Their absorption onsets, corresponding to the fundamental 0−0 transitions, are observed at 1050 nm for **4** and 830 nm for **6**.[29] The energy levels of the excited singlet states of **4** and **6** are accordingly derived as 1.2 and 1.5 eV, respectively.[30] The conjugates **3** and **5b**, on the other hand, exhibit additional features that relate to ZnP (i.e., **3**, maxima at 427, 556, and 596 nm; **5b**, maxima at 427, 555, and

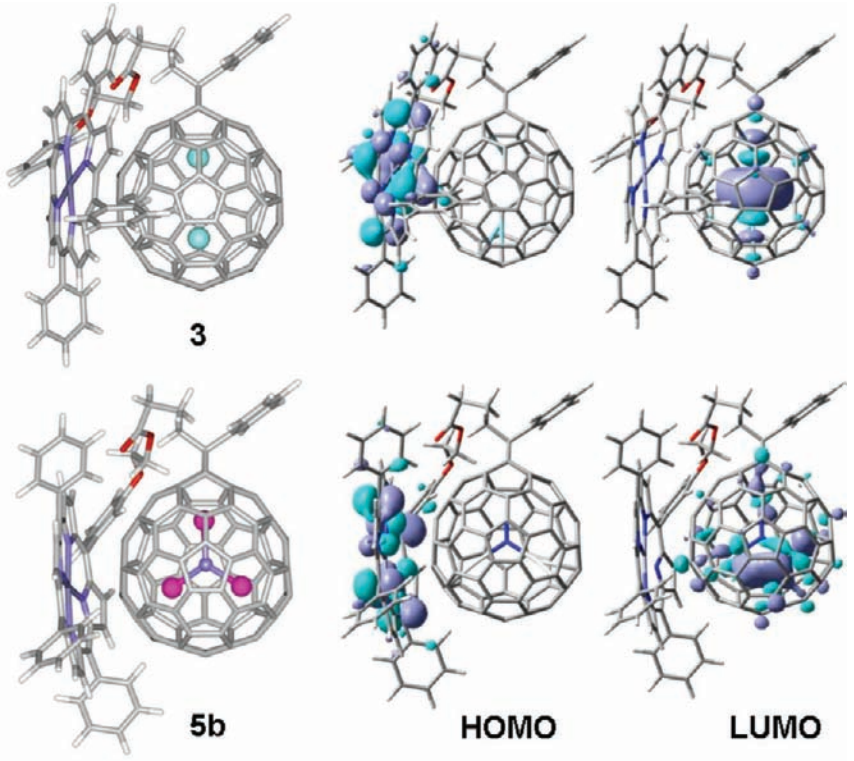

Figure 5. (Left panels) Optimized structures of **3** and **5b**; (central and right panels) HOMO and LUMO distributions (isosurface value 0.03 au).

dx.doi.org/10.1021/ja202331r |*J. Am. Chem. Soc.* 2011, 133, 7608–7618

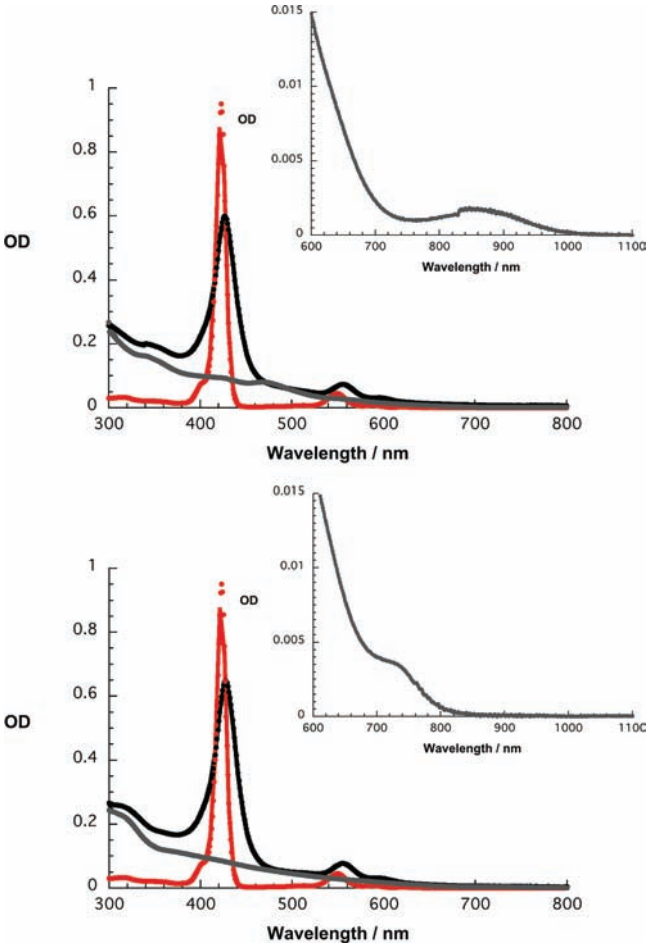

Figure 6. (Upper panel) Absorption spectra of **3** (black spectrum), **4** (grey spectrum), and ZnP (red spectrum) as reference in toluene with the inset showing the absorption onset in **3**. (Lower panel) Absorption spectra of **5b** (black spectrum), **6** (grey spectrum), and ZnP (red spectrum) as reference in toluene with the inset showing the absorption onset in **5b**.

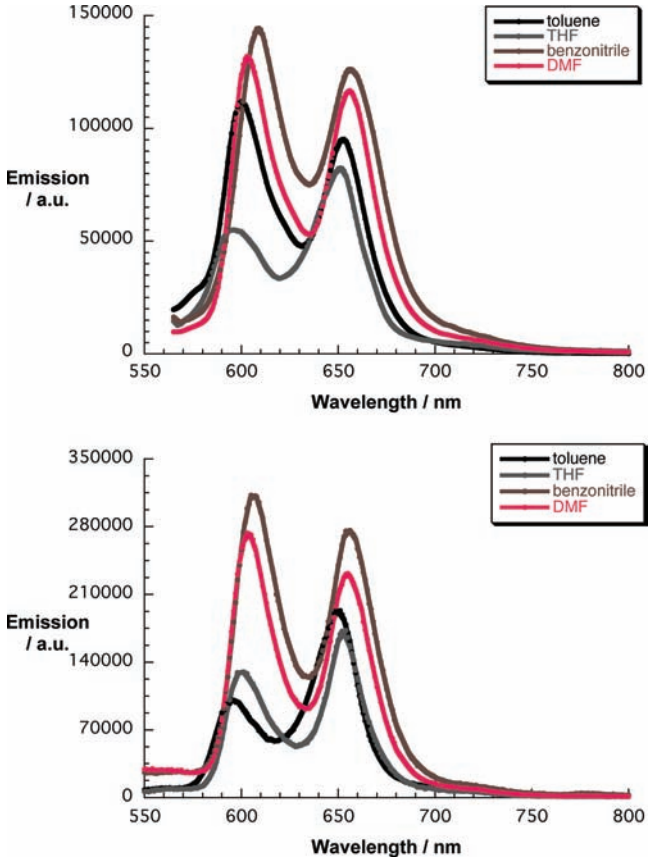

Figure 7. (Upper panel) Room temperature steady-state fluorescence spectra of **3** in solvents of different polarities, upon excitation at 554 nm. (Lower panel) Room temperature steady-state fluorescence spectra of **5b** in solvents of different polarities, upon excitation at 554 nm.

594 nm). Notable is, however, that the resulting absorption spectra fail to be simple superimpositions of the individual components. In particular, relative to ZnP (i.e., Soret-band maxima at 423 as well as Q-band maxima at 550 and 587 nm), the Soret bands in **3** and **5b** appear much broader. In fact, upon subtracting the metallofullerene absorptions, significantly weaker Soret bands emerge for **3** (5.49 (log ε)) and **5b** (5.53 (log ε)) relative to ZnP (5.76 (log ε)). Moreover, the Soret- and the Q-bands are red-shifted by 4, 6, and 9 nm for **3** as well as 4, 5, and 7 nm for **5b**. Taken the aforementioned into concert, we postulate appreciable electronic interactions between the two constituents in **3** and **5b**, that is, a redistribution of electron density.

To understand the electronic interactions between ZnP and the metallofullerenes in the excited states, emission measurements were carried out with **3** and **5b** in solvents of different polarity, toluene, THF, benzonitrile, and DMF. Figure 7 attests that both **3** and **5b** displayed ZnP centered emissions with maxima at 605 and 650 nm. When, however, compared to pristine ZnP, the ZnP fluorescence is significantly quenched in all solvents. To this end, quantum yields ranging from 10^{-3} to 10^{-4} prompt to efficient deactivation pathways, beyond the intrinsic pathways of radiative and nonradiative recovery of the singlet ground state or intersystem crossing , such as electron or energy transfer.

Decisive insights into the mechanism, by which photoexcited **3** and **5b** deactivate, came from transient absorption measurements. Herein, all of the compounds were probed upon femtosecond laser excitation at, for example, 387 nm excitation, which ensures the photoexcitation of both ZnP and metallofullerene units. First, the excited state features of **4** were monitored, see Figure S17. Immediately after the laser excitation, a broad transient is detected that covers most of the near-infrared region (i.e., 900−1200 nm) and bears considerable resemblance with that seen for $La_2@C_{80}$[15d] and can be assigned to the singlet excited state of $La_2@C_{80}$. Along with the decay of the singlet excited state of $La_2@C_{80}$, a new maximum gradually emerged at 580 nm. In fact, a lifetime exceeding 3000 ps suggests formation of the energetically lower-lying triplet excited state of $La_2@C_{80}$ through intersystem crossing. The singlet excited state lifetime was estimated to be around 30 ps from the decay of the singlet signature in the red and the growth of the triplet signature in the blue. Such a lifetime is, on one hand, comparable to that of $Sc_3N@C_{80}$ (i.e., 48 ps), but, on the other hand, nearly 2 orders faster than that of the C_{60} analogue (i.e., 1.25 ns).[31] An "endohedral heavy-atom effect" is likely to be responsible for the ultrafast singlet excited state decay.[32]

The transient absorption spectra of **3** in toluene and THF are shown in Figure 8. At early times, the transients are virtually

dx.doi.org/10.1021/ja202331r |*J. Am. Chem. Soc.* 2011, 133, 7608–7618

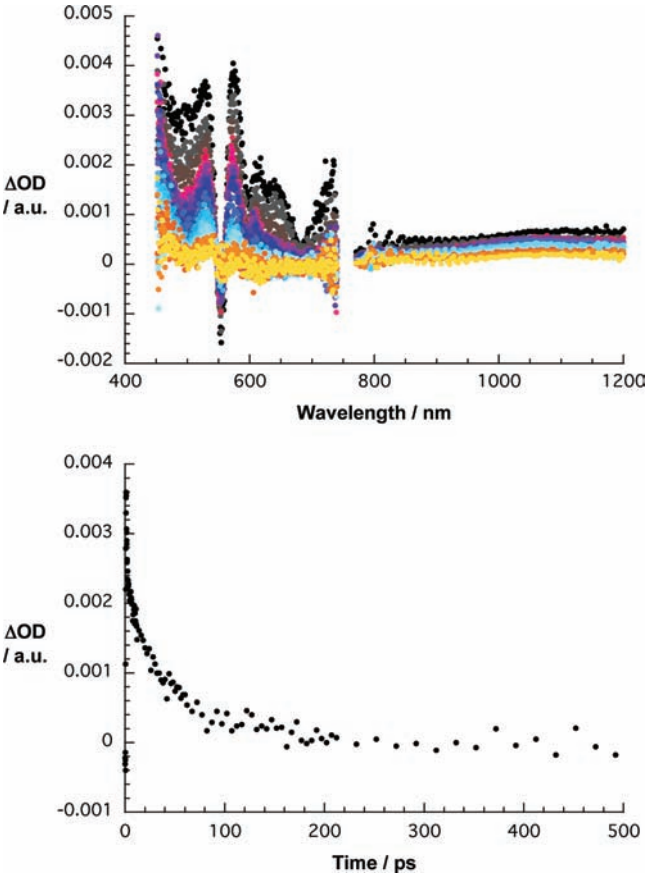

Figure 8. (Upper panel) Differential absorption spectra (visible and near-infrared) obtained upon femtosecond flash photolysis (387 nm) of **3** ($\sim 10^{-5}$ M) in argon saturated toluene with several time delays between 0 and 150 ps at room temperature; time progression from black and red to blue and orange. (Lower panel) Time-absorption profile of the spectra shown above at 530 nm, monitoring the charge separation and charge recombination dynamics.

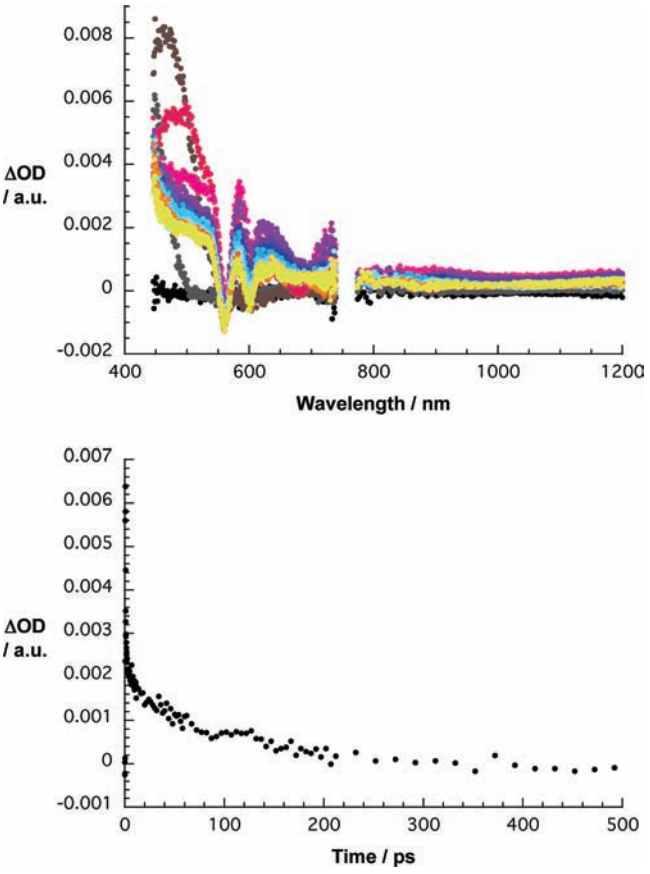

Figure 9. (Upper panel) Differential absorption spectra (visible and near-infrared) obtained upon femtosecond flash photolysis (387 nm) of **3** ($\sim 10^{-5}$ M) in argon saturated DMF with several time delays between 0 and 10 ps at room temperature; time progression from black and red to blue and orange. (Lower panel) Time-absorption profile of the spectra shown above at 500 nm, monitoring the charge separation and charge recombination dynamics.

identical to those seen for pristine ZnP,[16] indicating the instantaneous formation of the ZnP singlet excited state despite the presence of $La_2@C_{80}$. Nevertheless, after short time delays (i.e., 1 ps), new transient features start to develop in the visible range, including maxima between 580 and 700 nm. Important is the close resemblance with the one-electron oxidized form of ZnP.[33] When turning to the near-infrared range, a broad and nevertheless weak absorption centered around 1000−1200 nm is seen, which relates to the one-electron reduced form of $La_2@C_{80}$.[34] Thus, our spectroscopic analyses corroborate that the fast deactivation of the ZnP singlet excited state (i.e., $>10^{12}$ s^{-1}) results in the formation of the $(La_2@C_{80})^{\bullet-}-(ZnP)^{\bullet+}$ radical ion pair state. The $(La_2@C_{80})^{\bullet-}-(ZnP)^{\bullet+}$ radical ion pair state decays, at 640 nm ($ZnP^{\bullet+}$) and 1050 nm ($La_2@C_{80}^{\bullet-}$), were best fitted by monoexponential fitting functions. From the latter analyses, lifetimes 230 ps in toluene and 170 ps THF were derived. Notable is the lack of any transient that relates to either the ZnP or the $La_2@C_{80}$ triplet excited state (i.e., at 840 or 580 nm), which corroborates that the $(La_2@C_{80})^{\bullet-}-(ZnP)^{\bullet+}$ radical ion pair state recombines directly to the ground state.

A closer inspection of the transient absorption changes seen in benzonitrile and DMF reveals characteristics that differ from those seen in toluene and THF. Figure 9 demonstrates, for example, that in the visible region new minima and maxima develop at 560/600 nm and 495/580/640 nm, respectively. An apparent mismatch emerges relative to the features known for the one-electron oxidized ZnP. This led us to revisit our spectroelectrochemical investigations and to probe the cathodic range, that is, applying a potential of −1.5 V (vs SCE) to reduce ZnP.[16] In fact, the corresponding spectral changes are an exact match of what was observed during the femtosecond transient absorption measurements. Likewise, in the near-infrared, only anodic conditions in the spectroelectrochemistry led to an agreement with the femtosecond transient absorption measurements, that is, a maximum at 870 nm. The time absorption profiles indicate that the $(La_2@I_h\text{-}C_{80})^{\bullet+}-(ZnP)^{\bullet-}$ radical ion pair is metastable. In fact, multiwavelength analyses provide lifetimes of 108 and 62 ps in benzonitrile and DMF, respectively.

Next, excitation of **6** at 387 nm populates its singlet excited state with characteristic absorption maxima at 500 and 1100 nm, see Figure S18. The latter undergoes intersystem crossing to the corresponding triplet manifold with a characteristic lifetime exceeding 3000 ps and a characteristic maximum at 590 nm.

Upon photoexciting **5b**, the ZnP centered singlet excited state decays rapidly. As Figure 10 illustrates, the ZnP singlet excited state features transform over the course of 10 ps. Moreover, the fast decay is associated with marked changes in the differential

dx.doi.org/10.1021/ja202331r |*J. Am. Chem. Soc.* 2011, 133, 7608–7618

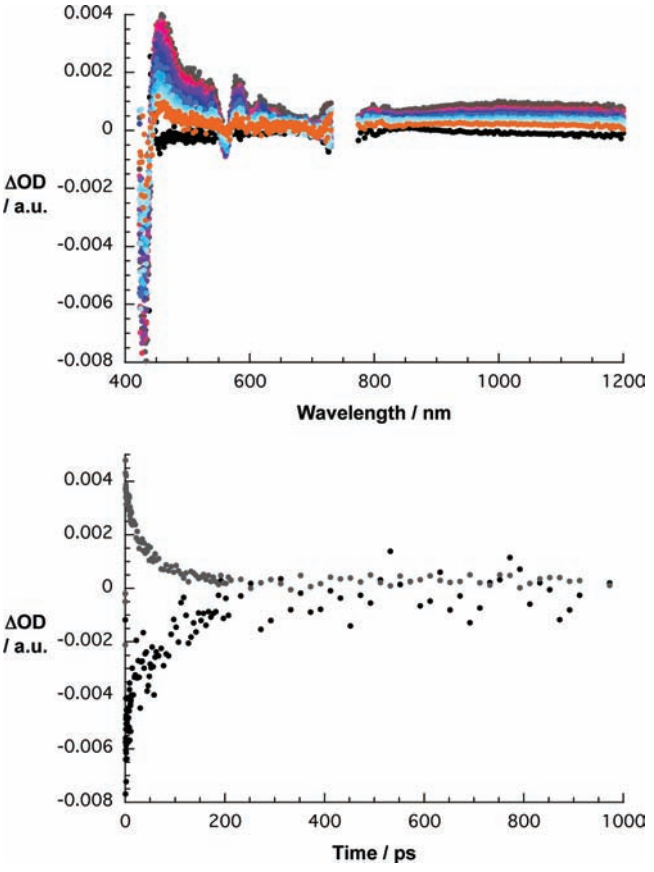

Figure 10. (Upper panel) Differential absorption spectra (visible and near-infrared) obtained upon femtosecond flash photolysis (387 nm) of **5b** ($\sim 10^{-5}$ M) in argon saturated THF with several time delays between 0 and 150 ps at room temperature; time progression from black and red to blue and orange. (Lower panel) Time-absorption profiles of the spectra shown above at 435 and 460 nm, monitoring the charge separation and charge recombination dynamics.

absorption spectrum, a new set of maxima which evolve in the visible region (i.e., 580−700 nm) as well as in the near-infrared region (i.e., 1000 nm). Of particular importance is the close resemblance of the near-infrared part with the radiolytically and spectroelectrochemically generated spectrum of the one-electron reduced $Sc_3N@C_{80}$ radical anion. In the visible portion, features of the one-electron oxidized form of ZnP evolve around 680 nm. Taking this into consideration, we conclude the successful formation of the radical ion pair state. Importantly, unlike **3**, experiments with **5b** in benzonitrile reveal no change in charge transfer product. In other words, the same $(Sc_3N@C_{80})^{\bullet-}-(ZnP)^{\bullet+}$ radical ion pair state is formed regardless of the solvent polarity. Kinetically, the time-absorption profiles in Figure 10 also corroborate that the radical ion pair state is metastable, namely, decaying with a lifetime of 42 ps in toluene and 49 ps in benzonitrile. Spectroscopically, the product of charge recombination is, however, not the ground state, but the triplet excited state of $Sc_3N@C_{80}$ (1.2 eV) with its 590 nm fingerprint. Independent confirmation for this hypothesis came from a consideration of the associated energy levels, vide infra.

CONCLUSION

In summary, novel $La_2@C_{80}$−ZnP (**3**) and $Sc_3N@C_{80}$−ZnP (**5b**) conjugates have been synthesized, both of which are featured by a common (6,6)-open addition pattern. Notable, past work has demonstrated the intrinsic instability of $Sc_3N@C_{80}$ based electron donor−acceptor conjugates. Despite these limitations, we succeed in the synthesis, isolation, and investigation of a $Sc_3N@C_{80}$ electron donor−acceptor conjugate that bears a ZnP as excited state electron donor. Structural characterizations suggest, however, a more restricted conformation for **3**, while a somewhat conformational flexibility for **5b**, probably owing to the presence of the standing La_2 cluster in **3** and the 2D-rotated Sc_3N cluster in **5b**. DFT-calculations reveal a slightly closer proximity between the two entities of **3** as compared to that of **5b**. Their geometrical conformations and LUMO distributions, at our applied computational level, are also sensitive to the type of endohedral clusters. Moreover, it is important to note that electrochemical and absorption assays evidence a significant intramolecular ground-state interaction in **3**, whereas such interaction is less pronounced in **5b**.

In the excited state, that is, upon photoexciting either $La_2@C_{80}$/$Sc_3N@C_{80}$ or ZnP, both conjugates show a considerable charge transfer activity. For example, **3** undergoes, upon photoexcitation, a fast charge separation process and yields a radical ion pair, whose nature, namely $(La_2@C_{80})^{\bullet-}-(ZnP)^{\bullet+}$ versus $(La_2@C_{80})^{\bullet+}-(ZnP)^{\bullet-}$, varies with solvent polarity. **5b**, on the other hand, afforded the same $(Sc_3N@C_{80})^{\bullet-}-(ZnP)^{\bullet+}$ radical ion pair regardless of the solvent.

Such change in photoreactivity is easily rationalized when considering the corresponding energy levels in **3** and **5b** as we have derived them from the electrochemical assays. In particular, the $(La_2@C_{80})^{\bullet-}-(ZnP)^{\bullet+}$ radical ion pairs in **3** were estimated to have energy levels of 0.72 eV in toluene, 0.52 eV in THF, 0.46 eV in benzonitrile, and 0.45 eV in DMF.[35] In other words, charge separation evolving from the ZnP singlet excited state (2.0 eV) is thermodynamically feasible in any of the tested solvents. On the contrary, the $(La_2@C_{80})^{\bullet+}-(ZnP)^{\bullet-}$ radical ion pair state energies are 2.3 eV in toluene, 2.1 eV in THF, 2.0 eV in benzonitrile, and in DMF, which renders charge separation from the ZnP singlet excited state thermodynamically only feasible in the more polar solvents, namely benzonitrile and DMF.

A fundamentally different picture evolves for **5b**. In line with the experimental results, only the $(Sc_3N@C_{80})^{\bullet-}-(ZnP)^{\bullet+}$ radical ion pair formation is exothermic with energies of 1.74 eV in toluene, 1.53 eV in THF, 1.46 eV in benzonitrile, and 1.45 eV in DMF. A $(Sc_3N@C_{80})^{\bullet+}-(ZnP)^{\bullet-}$ radical ion pair is unlikely to be formed due to thermodynamically uphill processes, that is, from 2.0 eV for the ZnP singlet excited state to charge separation state that is about 2.2−2.5 eV in DMF and toluene, respectively.

EXPERIMENTAL SECTION

General. All chemicals were of reagent grade and purchased from Wako. They were used as received unless specified. *o*-Dichlorobenzene was distilled over CaH_2 and stored with 4 Å molecular sieve. $La_2@I_h$-C_{80} and $Sc_3N@I_h$-C_{80} were produced and separated according to previously reported method. Analysis and preparative HPLC were performed on Buckyprep column, 5PYE column, Buckyclutcher column (ø4.6 × 100 mm, Cosmosil) and preparative Buckyprep column (ø25 × 100 mm, Cosmosil), respectively. Toluene was used as eluent. All NMR spectra were recorded on a Bruker AC 300 spectrometer or Bruker AV 500 spectrometer with a CryoProbe system, locked on deuterated solvents and referenced to the solvent peak. The 1D (^{1}H, ^{13}C, dept135) and 2D experiments (COSY, DQF-COSY, HMQC) were performed by means

dx.doi.org/10.1021/ja202331r |*J. Am. Chem. Soc.* 2011, 133, 7608–7618

of standard experimental procedures of the Bruker library. Matrix-assisted laser desorption-ionization time-of flight (MALDI-TOF) mass spectra were recorded with a Bruker BIFLEX-III mass spectrometer (λ = 337 nm) using 1,1,4,4-tetraphenyl-1,3-butadiene as the matrix. The measurements were performed in both positive and negative ion modes.

Theoretical Calculations. The calculations were carried out using the hybrid density functional theory (DFT) at the M06-2X level[27] with the relativistic effective core potential as implemented in the *Gaussian 09* software package. The LANL2DZ basis set was employed for La, Sc and Zn and 3-21G(d) basis set for C, H, O, N.[36]

Absorption and Steady-State Emission. The UV−vis experiments were carried out on a Varian Cary 5000 UV−vis-NIR spectrophotometer. The fluorescence studies were performed on a Fluoromax 3 (Horiba) using 554 nm as excitation wavelength. The measurements were carried out at room temperature.

Photophysical Studies. Femtosecond transient absorption studies were performed using the 387 nm laser pulses of 150 fs pulse width, generated by a β-Barium borate crystal upon higher order nonlinear processes from an amplified Ti:Sapphire laser system (CPA 2001 Laser, Clark-MXR Inc.) The white light was generated by a 2 mm Sapphire Crystal and with the help of a delay line, a time delay between the pump and the probe beams were created with a high precision. Finally, the change in optical density (ΔOD) is measured against the wavelength in both visible and near-infrared regions. Nanosecond laser flash photolysis experiments were performed with 337-nm laser pulses from a nitrogen laser (8-ns pulse width) in front face excitation geometry.

Radiolysis. Pulse radiolysis experiments were performed using 50 ns pulses of 15 MeV electrons from a linear electron accelerator (LINAC). Dosimetry was based on the oxidation of SCN^- to $(SCN)_2^{\bullet-}$ which in aqueous, N_2O-saturated solution takes place with G $\approx$ 6 (G denotes the number of species per 100 eV, or the approximate μM concentration per 10 J absorbed energy). The radical concentration generated per pulse was varied between $(1-3) \times 10^{-6}$ M.

Electrochemistry. Differential pulse voltammetry (DPV) and cyclic voltammetry (CV) were carried out in *o*-DCB under Ar atmosphere at room temperature using a BAS CW-50 instrument. A conventional three-electrode cell consisting of a platinum working electrode, a platinum counter-electrode, and a saturated calomel reference electrode (SCE) was used for both measurements. $(n\text{-Bu})_4NPF_6$ was used as the supporting electrolyte. All potentials were recorded against a SCE reference electrode and corrected against Fc/Fc^+. DPV and CV were measured at a scan rate of 20 and 100 mV s^{-1}, respectively.

Synthesis. *1-(3-(Methoxycarbonyl)propyl)-1-phenyl-[6,6]La_2@C_{81} (**4**).* Methyl 4-benzoylbutyrate *p*-tosylhydrazone (1.4 mg, 3.7 μmol) and a small amount of NaOMe were dissolved in 60 μL of dry pyridine under Ar for 10 min. A solution of 1.5 mg of La_2@C_{80} (1.2 μmol) in 2.5 mL of *o*-DCB was added, and the mixture was stirred at 75 °C for 2 h. After cooling to room temperature, solvents were removed under vacuum. Then, a solution of CS_2/acetone (v/v = 1:1) with 3−4 μL of $CHCl_2COOH$ was added to dissolve the solid. The mixture was stirred for 15 min. The resulting mixture was separated by HPLC and **4** was isolated as predominant product. Yield: 55% based on consumed La_2@C_{80}. ^{1}H NMR (300 MHz, $C_2D_2Cl_4$): δ = 8.84 (d, ^2J = 7.60 Hz, 1H, *o*-ArH), 8.29 (d, ^2J = 7.60 Hz, 1H, *o*-ArH), 7.76 (t, ^3J = 7.50 Hz, 1H, *m*-ArH), 7.70 (t, ^3J = 7.50 Hz, 1H, *m*-ArH), 7.59 (t, ^3J = 7.50 Hz, 1H, *p*-ArH), 3.69 (s, 3H, OCH_3), 3.56 (br, $1H_\alpha$, $PhCCH_2CH_2$), 3.46 (br, $1H_\beta$, $PhCCH_2CH_2$), 2.66 (t. ^3J = 6.50 Hz, 2H, CH_2CH_2CO), 2.61 (br., $1H_\alpha$, $PhCCH_2CH_2$), 2.49 (br, $1H_\beta$, $PhCCH_2CH_2$). ^{13}C NMR (125 MHz, $C_2D_2Cl_4$): δ = 172.63 (C═O), 153.84, 153.78, 151.47, 151.39, 151.05, 150.89, 150.45, 150.42, 150.39, 149.93, 149.86, 149.44, 149.25, 148.05, 147.45, 147.38,146.46, 146.39, 145.37, 145.32, 145.19, 144.97, 144.27, 144.11, 144.09, 143.59, 143.58, 143.06, 142.94, 142.86, 141.40, 141.27, 140.96, 140.19, 140.16, 137.69, 137.66, 137.54, 137.52, 137.50, 137.48, 137.46, 137.29, 137.21, 137.20, 137.17, 136.96, 135.08, 134.95, 134.74, 134.72, 134.71, 134.66, 134.55, 134.29, 134.26, 134.22, 134.16, 133.00, 132.23, 131.94, 131.79, 130.83, 130.69, 130.35 (Ar), 129.43 (Ar), 129.18 (Ar), 129.15 (Ar), 128.82 (Ar), 127.16, 125.69, 124.84, 121.79, 120.15, 107.00, 93.29, 51.74 (OCH_3), 49.08 (spiro *C*), 41.76 ($PhCCH_2$), 34.08 (CH_2CO_2), 20.60 ($CH_2CH_2CO_2$). MS (MALDI-TOF): *m/z* = 1429.90 $[M + 2H]^+$; Calcd for $La_2C_{92}H_{14}O_2$: *m/z* = 1427.90.

*La_2@I_h-C_{80}−ZnP (**3**).* H_2P diazo precursor (4.5 mg, 4.1 μmol) and a small amount of NaOMe were dissolved in pyridine (150 μL) and stirred for 15 min under Ar. Then, La_2@C_{80} (1.13 mg, 0.91 μmol) in 1.5 mL of *o*-DCB was added in. The mixture was stirred at 80 °C for 2 h under Ar. After cooling down the reaction mixture, 500 μL of saturated $Zn(OAc)_2$/MeOH was added, and the mixture was stirred for 30 min. After removing the solvent under vacuum, the solid was dissolved in toluene and filtered. The final reaction mixture was subject to HPLC analysis. **3** was facilely separated and purified by two-step HPLC process. Yield: 45% based on consumed La_2@C_{80}. ^{1}H NMR (500 MHz, $C_2D_2Cl_4$): δ = 8.92 (d, ^2J = 4.63 Hz, 1H-β), 8.89 (d, ^2J = 4.65 Hz, 1H-β), 8.83 (d, ^2J = 4.68 Hz, 1H-β), 8.79 (d, ^2J = 4.65 Hz, 2H-β overlapped), 8.77 (d, ^2J = 4.61 Hz, 1H-β), 8.72 (t, 2H-β overlapped), 8.53 (d, ^2J = 7.62 Hz, 1H-*Ar*), 8.21 (d, ^2J = 7.68 Hz, 1H-*Ar*), 8.18 (d, ^2J = 6.07 Hz, 1H-*Ar*), 8.15 (d, ^2J = 6.17 Hz, 1H-*Ar*), 8.04 (d, ^2J = 7.39 Hz, 1H-*Ar*), 7.98 (d, ^2J = 6.87 Hz, 1H-*Ar*), 7.89 (d, ^2J = 7.27 Hz, 1H-*Ar*), 7.80−7.63 (m, 12H), 7.59−7.50 (m, 7H), 7.30 (d, ^2J = 7.74 Hz, 1H-*Ar*), 4.52 (t, ^2J = 3.60 Hz, 2H, $PhOCH_2$), 4.31 (br, 2H, $PhOCH_2CH_2$), 3.25 (br, $1H_\alpha$, $PhCCH_2CH_2$), 3.18 (br, $1H_\beta$, $PhCCH_2CH_2$), 2.62 (t. ^3J = 6.30 Hz, 2H, CH_2CH_2CO), 2.40 (br., $1H_\alpha$, $PhCCH_2CH_2$), 2.27 (br, $1H_\beta$, $PhCCH_2CH_2$). ^{13}C NMR (125 MHz, $C_2D_2Cl_4$): δ = 173.20 (C═O), 156.99, 151.41, 151.14, 150.54, 150.53, 150.45, 150.40, 150.38, 150.35, 150.21, 150.20, 149.93, 149.81, 149.59, 149.21, 148.68, 148.33, 148.28, 148.03, 147.90, 147.64, 147.50, 146.47, 145.62, 145.59, 145.44, 144.96, 144.77, 144.32, 144.24, 144.20, 144.10, 143.32, 143.15, 143.07, 143.05, 142.87, 142.77, 142.70, 142.58, 142.37, 141.58, 139.89, 139.68, 139.38, 138.68, 138.42, 138.38, 137.15, 136.95, 136.91, 136.81, 136.75, 136.37, 136.34, 136.24, 136.15, 135.90, 135.37, 134.80, 134.63, 134.35, 134.26, 133.96, 133.94, 133.92, 133.88, 133.79, 133.74, 133.67, 133.39, 133.15, 132.85, 132.21, 132.17, 132.13, 131.99, 131.88, 131.60, 131.38, 131.24, 130.36, 130.29, 129.47, 129.32, 129.24, 129.18, 129.16, 128.87, 128.75, 127.88, 127.72, 127.63, 127.61, 127.11, 127.07, 127.01, 126.94, 126.82, 126.80, 126.43, 125.13, 124.25, 123.97, 122.49, 121.49, 121.45, 121.40, 121.13, 120.58, 119.52, 113.03, 106.56, 93.00, 66.26 (OCH_2), 63.53 (CH_2OCO), 48.87 (spiro *C*), 41.01 ($PhCCH_2$), 34.49 (CH_2CO_2), 20.74 ($CH_2CH_2CO_2$). MS (MALDI-TOF): *m/z* = 2134.57 $[M + 2H]^+$; Calcd for $La_2C_{137}H_{42}N_4O_3Zn$: *m/z* = 2132.07.

*Sc_3N@I_h-C_{80}-ZnP (**5b**).* H_2P diazo precursor (4.5 mg, 4.1 μmol) and a small amount of NaOMe were dissolved in pyridine (150 μL) and stirred for 15 min under Ar. Then, Sc_3N@I_h-C_{80} (1.50 mg, 1.35 μmol) in 2 mL of *o*-DCB was added. The mixture was stirred at 80 °C for over 20 h under Ar. Sc_3N@I_h-C_{80}−H_2P (**5a**) was separated as the second fraction and purified by two-step HPLC process. Yield: 78% based on consumed Sc_3N@I_h-C_{80}. Sc_3N@I_h-C_{80}−H_2P (1 mg, 0.52 μmol) was dissolved in 5 mL of *o*-DCB. A saturated methanol solution of $Zn(OAc)_2$ (500 μL) was added and the mixture was stirred for 30 min. After removing the solvent under vacuum, the solid was dissolved in toluene and filtered. Sc_3N@I_h-C_{80}−ZnP (**5b**) was purified by HPLC. The conversion yield was over 90%. **Sc_3N@I_h-C_{80}-H_2P (5a)**: ^{1}H NMR (500 MHz, $C_2D_2Cl_4$): δ = 8.83−8.78 (m, 8H-β), 8.30−8.25 (m, 3H), 8.06 (br, s, 1H), 7.99 (d, ^2J = 6.87 Hz, 2H), 7.91 (d, ^2J = 6.78 Hz, 1H), 7.71−7.65 (m, 12H), 7.59 (br, s, 2H), 7.29 (m, 4H), 4.46 (br, 2H, $PhOCH_2$), 4.30 (br, m, 2H, $PhOCH_2CH_2$), 2.40 (br, 2H, $PhCCH_2CH_2$), 2.34 (br, 2H, CH_2CH_2CO), 1.74 (br. 2H, $PhCCH_2CH_2$), −3.00 (s, 2H, *NH*). ^{13}C NMR (125 MHz, $C_2D_2Cl_4$): δ = 173.12 (C═O), 157.05, 151.11, 150.83, 150.73, 150.35, 149.31, 149.12, 149.08, 147.88, 147.60, 147.17, 146.83, 146.64, 145.87, 145.14, 144.80, 144.78, 144.40, 144.16, 144.07, 144.01, 143.93, 143.76, 142.88, 142.74, 142.71,

142.69, 142.66, 142.47, 142.34, 142.32, 142.15, 142.06, 141.79, 141.69, 141.55, 141.36, 141.26, 141.10, 140.86, 140.68, 140.48, 140.46, 140.39, 140.16, 140.09, 139.90, 139.48, 139.12, 138.65, 138.28, 138.10, 137.91, 137.49, 136.56, 136.20, 135.58, 135.44, 135.05, 135.00, 134.86, 134.84, 134.77, 134.47, 133.89, 133.83, 133.50, 133.46, 133.33, 133.19, 129.22, 128.86, 128.79, 128.54, 128.25, 128.08, 128.03, 127.47, 127.31, 127.09, 126.91, 126.88, 124.68, 123.37, 122.55, 122.13, 121.78, 120.93, 120.82, 119.94, 113.93, 95.77, 95.10, 66.34 ($PhOCH_2$), 63.38 (CH_2OCO), 48.79 (spiro *C*), 37.66 ($PhCCH_2$), 34.23 (CH_2CO_2), 20.46 ($CH_2CH_2CO_2$). MS (MALDI-TOF): m/z = 1942.43 $[M + H]^+$; Calcd for $Sc_3C_{137}H_{44}N_5O_3$: m/z = 1941.22. **$Sc_3N@I_h$-C_{80}-ZnP (5b)**: ^{1}H NMR (500 MHz, $C_2D_2Cl_4$): δ = 8.91−8.83 (br, m, 8H-β), 8.22 (br, 2H), 8.00 (br, 1H), 7.93 (br, m, 2H), 7.70−7.56 (br, m, 15H), 7.33 (br, m, 2H), 7.27 (br, m, 2H), 4.46 (br, 2H, $PhOCH_2$), 4.31−4.27 (br, m, 2H, $PhOCH_2CH_2$), 2.37 (t, ^3J = 7.90 Hz, 2H, $PhCCH_2CH_2$), 2.33 (t, ^3J = 6.00 Hz, 2H, CH_2CH_2CO), 1.74 (br. 2H, $PhCCH_2CH_2$). MS (MALDI-TOF): m/z = 2004.04 $[M + H]^+$; Calcd for $Sc_3C_{137}H_{42}N_5O_3Zn$: m/z = 2003.13.

■ ASSOCIATED CONTENT

Supporting Information. Synthesis schemes. HPLC profiles of the isolated **3**−**5**. MALDI-TOF spectra of **3**−**5**. H−H (DQF)COSY spectrum of **3** and **4**. ^{13}C NMR and DEPT 45/135 spectrum for **3**, **4** and $Sc_3N@C_{80}$-H_2P. Cyclic voltammograms (CV) of **3**−**6**. Transient absorption spectra of **3** in THF. This material is available free of charge via the Internet at http://pubs.acs.org.

■ AUTHOR INFORMATION

Corresponding Author
akasaka@tara.tsukuba.ac.jp; nagase@ims.ac.jp; dirk.guldi@chemie.uni-erlangen.de

■ ACKNOWLEDGMENT

This work is supported in part by a Grant-in-Aid for Scientific Research on Innovative Areas (No. 20108001, "pi-Space"), a Grant-in-Aid for Scientific Research (A) (No. 20245006), The Next Generation Super Computing Project (Nanoscience Project), Nanotechnology Support Project, a Grant-in-Aid for Scientific Research on Priority Area (Nos. 20036008, 20038007), and Specially Promoted Research from the Ministry of Education, Culture, Sports, Science, and Technology of Japan and The Strategic Japanese-Spanish Cooperative Program funded by JST and MICINN. H.N. thanks the Japan Society for the Promotion of Science (JSPS) for the Research Fellowship for Young Scientists. Financial support was also provided by the Ministry of Spain (Projects CTQ2008-00795/BQU and Consolider-Ingenio 2010C-07-25200), CAM (MADRISOLAR Project P-PPQ-000225-0505). D.M.G. acknowledges financial support from the Deutsche Forschungsgemeinschaft - GU 517/14-1 and - Cluster of Excellence (EAM).

■ REFERENCES

(1) (a) Grätzel, M. *Acc. Chem. Res.* **2009**, *42*, 1788–1798. (b) Delgado, J. L.; Bouit, P.-A.; Filippone, S.; Herranz, M. A.; Martín, N. *Chem. Commun.* **2010**, *46*, 4853–4865.

(2) Gust, D.; Moore, T. A.; Moore, A. L. *Acc. Chem. Res.* **2009**, *42*, 1890–1898.

(3) Heremans, P.; Cheyns, D.; Rand, B. P. *Acc. Chem. Res.* **2009**, *42*, 1740–1747.

(4) Ferraris, J. P.; Cowan, D. O.; Walatka, V.; Perilstein, J. H. *J. Am. Chem. Soc.* **1973**, *95*, 948–949.

(5) Tang, C. W. *Appl. Phys. Lett.* **1986**, *48*, 183–185.

(6) (a) Imahori, H.; Sakara, Y. *Eur. J. Org. Chem.* **1999**, *10*, 2445–2457. (b) Guldi, D. M.; Gouloumis, A.; Vázquez, P.; Torres, T.; Georgakilas, V.; Prato, M. *J. Am. Chem. Soc.* **2005**, *127*, 5811–5813. (c) de la Escosura, A.; Martínez-Diaz, M. V.; Guldi, D. M.; Torres, T. *J. Am. Chem. Soc.* **2006**, *128*, 4112–4118. (d) Zeng, H.-P.; Wang, T.; Sandanayaka, A. S. D.; Araki, Y.; Ito, O. *J. Phys. Chem.A* **2005**, *109*, 4713–4720. (e) D'Souza, F.; Chitta, R.; Gadde, S.; Islam, D.-M. S.; Schumacher, A.; Zandler, M. E.; Araki, Y.; Ito, O. *J. Phys. Chem.B* **2006**, *110*, 25240–25250. (f) Gayathri, S. S.; Wielopolski, M.; Pérez, E. M.; Fernández, G.; Sánchez, L.; Viruela, R.; Ortí, E.; Guldi, D. M.; Martín, N. *Angew. Chem., Int. Ed.* **2009**, *48*, 815.

(7) (a) Akasaka, T.; Nagase, S., Eds.; *Endofullerenes: A New Family of Carbon Cluster*; Kluwer: Dordrecht, The Netherlands, 2002. (b) Shinohara, H. *Rep. Prog. Phys.* **2000**, *63*, 843–892. (c) Yamada, M.; Akasaka, T.; Nagase, S. *Acc. Chem. Res.* **2010**, *43*, 92–102.(d) Feng, L.; Akasaka, T.; Nagase, S. . In *Carbon Nanotubes and Related Structures*; Guldi, D. M.; Martin, N., Eds.; Wiley-VCH: Weinheim, 2010; pp 455−490.

(8) (a) Bethune, D. S.; Johnson, R. D.; Salem, J. R.; de Vries, M. S.; Yannoni, C. S. *Nature* **1993**, *366*, 123–128. (b) Kobayashi, K.; Nagase, S.; Akasaka, T. *Chem. Phys. Lett.* **1995**, *245*, 230–236. (c) Kobayashi, K.; Nagase, S. *Chem. Phys. Lett.* **1996**, *262*, 227–232. (d) Kobayashi, K.; Nagase, S. *Chem. Phys. Lett.* **1998**, *282*, 325–329.

(9) For studies on $La_2@I_h$-C_{80}, refer: (a) Suzuki, T.; Maruyama, Y.; Kato, T.; Kikuchi, K.; Nakao, Y.; Achiba, Y.; Kobayashi, K.; Nagase, S. *Angew. Chem.* **1995**, *107*, 1228; *Angew. Chem., Int. Ed. Engl.* **1995**, *34*, 1094–1096; (b) Akasaka, T.; Nagase, S.; Kobayashi, K.; Waelchli, M.; Yamamoto, K.; Funasaka, H.; Kako, M.; Hoshino, T.; Erata, T. *Angew. Chem.* **1997**, *109*, 1716; *Angew. Chem., Int. Ed. Engl.* **1997**, *36*, 1643–1645; (c) Nishibori, E.; Takata, M.; Sakata, M.; Taninaka, A.; Shinohara, H. *Angew. Chem.* **2001**, *113*, 3086; *Angew. Chem., Int. Ed.* **2001**, *40*, 2998–2999. (d) Kobayashi, K.; Nagase, S.; Maeda, Y.; Wakahara, T.; Akasaka, T. *Chem. Phys. Lett.* **2003**, *374*, 562–566. (e) Shimotani, H.; Ito, T.; Iwasa, Y.; Taninaka, A.; Shinohara, H.; Nishibori, E.; Takata, M.; Sakata, M. *J. Am. Chem. Soc.* **2004**, *126*, 364–369.

(10) For studies on $Sc_3N@I_h$-C_{80}, refer: (a) Stevenson, S.; Rice, G.; Glass, T.; Harich, K.; Cromer, F.; Jordan, M. R.; Craft, J.; Hadju, E.; Bible, R.; Olmstead, M. M.; Maitra, K.; Fisher, A. J.; Balch, A. L.; Dorn, H. C. *Nature* **1999**, *401*, 55–57. (b) Kobayashi, K.; Sano, Y.; Nagase, S. *J. Comput. Chem.* **2001**, *22*, 1353–1358. (c) Alvarez, L.; Pichler, T.; Georgi, P.; Schwieger, T.; Peisert, H.; Dunsch, L.; Hu, Z.; Knupfer, M.; Fink, J.; Bressler, P.; Mast, M.; Golden, M. S. *Phy. Rev. B* **2002**, *66*, 035107. (d) Campanera, J. M.; Bo, C.; Olmstead, M. M.; Balch, A. L.; Poblet, J. M. *J. Phys. Chem. A* **2002**, *106*, 12356–12364. (e) Elliott, B.; Yu, L.; Echegoyen, L. *J. Am. Chem. Soc.* **2005**, *127*, 10885–10888. (f) Cardona, C. M.; Elliott, B.; Echegoyen, L. *J. Am. Chem. Soc.* **2006**, *128*, 6480–6485. (g) Popov, A. A.; Dunsch, L. *J. Am. Chem. Soc.* **2008**, *130*, 17726–17742. (h) Valencia, R.; Rodríguez-Fortea, A.; Clotet, A.; Graaf, C.; Chaur, M. N.; Echegoyen, L.; Poblet, J. M. *Chem.—Eur. J.* **2009**, *15*, 10997–11009.

(11) For comparable studies on $La_2@I_h$-C_{80} and $Sc_3N@I_h$-C_{80}, see: (a) Iiduka, Y.; Ikenaga, O.; Sakuraba, A.; Wakahara, T.; Tsuchiya, T.; Maeda, Y.; Nakahodo, T.; Akasaka, T.; Kako, M.; Mizorogi, N.; Nagase, S. *J. Am. Chem. Soc.* **2005**, *127*, 9956–9957. (b) Wakahara, T.; Iiduka, Y.; Ikenaga, O.; Nakahodo, T.; Sakuraba, A.; Tsuchiya, T.; Maeda, Y.; Kako, M.; Akasaka, T.; Yoza, K.; Horn, E.; Mizorogi, N.; Nagase, S. *J. Am. Chem. Soc.* **2006**, *128*, 9919–9925. (c) Wakahara, T.; Yamada, M.; Takahashi, S.; Nakahodo, T.; Tsuchiya, T.; Maeda, Y.; Akasaka, T.; Kako, M.; Yoza, K.; Horn, E.; Mizorogi, N.; Nagase, S. *Chem. Commun.* **2007**, 2680–2682.

(12) Akasaka, T.; Suzuki, T.; Maeda, Y.; Ara, M.; Wakahara, T.; Kobayashi, K.; Nagase, S.; Kako, M.; Nakadaira, Y.; Fujitsuka, M.; Ito, O. *J. Org. Chem.* **1999**, *64*, 566–569.

(13) Berlin, A.; Zotti, G.; Zecchin, S.; Schiavon, G.; Vercelli, B.; Zanelli, A. *Chem. Mater.* **2004**, *16*, 3667–3676.

(14) (a) Larade, B.; Taylor, J.; Zheng, Q. R.; Mehrez, H.; Pomorski, P.; Guo, H. *Phy. Rev. B* **2001**, *64*, 195402. (b) Kobayashi, S.; Mori, S.; Iida, S.; Ando, H.; Takenobu, T.; Taguchi, Y.; Fujiwara, A.; Taninaka, A.; Shinohara, H.; Iwasa, Y. *J. Am. Chem. Soc.* **2003**, *125*, 8116–8117. (c) Pérez-Jiménez, A. J. *J. Phys. Chem. C* **2007**, *111*, 17640–17645. (d) Ross, R. B.; Cardona, C. M.; Guldi, D. M.; Gayathri, S. S.; Reese, M. O.; Kopidakis, N.; Peet, J.; Walker, B.; Bazan, G. C.; Van Keuren, E.; Holloway, B. C.; Drees, M. *Nat. Mater.* **2009**, *8*, 208–212.

(15) (a) Pinzón, J. R.; Plonska-Brzezinska, M. E.; Cardona, C. M.; Athans, A. J.; Sankaranarayanan, S. G.; Guldi, D. M.; Herranz, M. A.; Martin, N.; Torres, T.; Echegoyen, L. *Angew. Chem., Int. Ed.* **2008**, *47*, 4173–4176. (b) Pinzón, J. R.; Cardona, C. M.; Herranz, M. A.; Plonska-Brzezinska, M. E.; Palkar, A.; Athans, A. J.; Martín, N.; Rodríguez-Fortea, A.; Poblet, J. M.; Bottari, G.; Torres, T.; Sankaranarayanan, S. G.; Guldi, D. M.; Echegoyen, L. *Chem.—Eur. J.* **2009**, *15*, 864–877. (c) Pinzón, J. R.; Gasca, D. C.; Sankaranarayanan, S. G.; Bottari, T.; Guldi, D. M.; Echegoyen, L. *J. Am. Chem. Soc.* **2009**, *131*, 7727–7734. (d) Takano, Y.; Herranz, Á.; Martín, N.; Radhakrishnan, S. G.; Guldi, D. M.; Tsuchiya, T.; Nagase, S.; Akasaka, T. *J. Am. Chem. Soc.* **2010**, *132*, 8048–8055.

(16) Guldi, D. M.; Feng, L.; Radhakrishnan, S. G.; Nikawa, H.; Yamada, M.; Mizorogi, N.; Tsuchiya, T.; Akasaka, T.; Nagase, S.; Herranz, Á.; Martín, N. *J. Am. Chem. Soc.* **2010**, *132*, 9078–9086.

(17) (a) Perepichka, D. F.; Bryce, M. R. *Angew. Chem., Int. Ed.* **2005**, *44*, 5370–5373. (b) Martín, N.; Sánchez, L.; Herranz, M. A.; Illescas, B.; Guldi, D. M. *Acc. Chem. Res.* **2007**, *40*, 1015.

(18) (a) Martín, N.; Sánchez, L.; Illescas, B.; Pèrez, I. *Chem. Rev.* **1998**, *98*, 2527–2548. (b) Bendikov, M.; Wudl, F.; Perepichka, D. F. *Chem. Rev.* **2004**, *104*, 4891–4986.

(19) (a) Guldi, D. M. *Chem. Soc. Rev.* **2002**, *31*, 22–36. (b) Sandanayaka, A. S. D.; Ikeshita, K.-I.; Araki, Y.; Kihara, N.; Furusho, Y.; Takata, T.; Ito, O. *J. Mater. Chem.* **2005**, *15*, 2276–2287. (c) D' Souza, F.; Chitta, R.; Gadde, S.; Islam, D.-M. S.; Schumacher, A. L.; Zandler, M. E.; Araki, Y.; Ito, O. *J. Phys. Chem.* **2006**, *110*, 25240–25250. (d) Mateo-Alonso, A.; Sooambar, C.; Prato, M. *C. R. Chem.* **2006**, *9*, 944–951. (e) Fazio, M. A.; Durandin, A.; Tkachenko, N. V.; Niemi, M.; Lemmetyinen, H.; Schuster, D. I. *Chem.—Eur. J.* **2009**, *15*, 7698–7705.

(20) (a) Xiao, J.; Savina, M. R.; Martin, G. B.; Francis, A. H.; Meyerhoff, M. E. *J. Am. Chem. Soc.* **1994**, *116*, 9341–9342. (b) Boyd, P. D. W.; Reed, C. A. *Acc. Chem. Res.* **2005**, *38*, 235–242. (c) Guldi, D. M. *J. Phys. Chem. B* **2005**, *109*, 11432.

(21) Crystal data for **4**·2CS_2: $C_{94}H_{14}La_2O_2S_4$, M_r = 1581.11, black chip, 0.23 × 0.18 × 0.03 mm, monoclinic, space group $P2_1/c$, a = 14.612(5) Å, b = 11.033(5) Å, c = 33.094(3) Å, β = 99.129(5), V = 5268(5) Å^3, Z = 4; ρ_{calcd} = 1.994 gcm^{-3}, μ(MoK$_\alpha$) = 1.829 mm^{-1}, θ_{max} = 27.48, T = 120 K, 42784 total collected reflections, 11955 unique reflections, 1058 refined parameters, GOF = 1.080, R_1 = 0.094 and wR_2 = 0.234 for all data; R_1 = 0.079 for 9576 independent reflections ($I > 2.0\sigma(I)$), min./max. electron density 3.204/−2.200 eÅ^{-3}.

(22) Shu, C.; Xu, W.; Slebodnick, C.; Champion, H.; Fu, W.; Reid, J. E.; Azurmendi, H.; Wang, C.; Harick, K.; Dorn, H. C.; Gibson, H. W. *Org. Lett.* **2009**, *11*, 1753–1756.

(23) (a) Imahori, H.; Hagiwara, K.; Aoki, M.; Akiyama, T.; Taniguchi, S.; Okada, T.; Shirakawa, M.; Sakata, Y. *J. Am. Chem. Soc.* **1996**, *118*, 11771–11782. (b) Boyd, P. D. W.; Hodgson, M. C.; Rickard, C. E. F.; Oliver, A. G.; Chaker, L.; Brothers, P. J.; Bolskar, R. D.; Tham, F. S.; Reed, C. A. *J. Am. Chem. Soc.* **1999**, *121*, 10487–10495. (c) Schuster, D. I. *Carbon* **2000**, *38*, 1607–1614. (d) Schuster, D. I.; Jarowski, P. D.; Kirschner, A. N.; Wilson, S. R. *J. Mater. Chem.* **2002**, *12*, 2041–2047. (e) Pérez, E. M.; Martín, N. *Chem. Soc. Rev.* **2008**, *37*, 1512–1519. (f) Lembo, A.; Tagliatesta, P.; Cicero, D.; Leoni, A.; Salvatori, A. *Org. Biomol. Chem.* **2009**, *7*, 1093–1096.

(24) Sutton, L. R.; Scheloske, M.; Primer, K. S.; Hirsch, A.; Guldi, D. M.; Gisselbrecht, J. P. *J. Am. Chem. Soc.* **2004**, *126*, 10370–10381.

(25) Pinzón, J. R.; Zuo, T.; Echegoyen, L. *Chem.—Eur. J.* **2010**, *16*, 4864–4869.

(26) Frisch, M. J. *GAUSSIAN 09*, Revision A. 02; Gaussian Inc.: Wallingford, CT, 2009.

(27) (a) Zhao, Y.; Truhlar, D. G. *Theor. Chem. Acc.* **2008**, *120*, 215–241. (b) Zhao, Y.; Truhlar, D. G. *J. Chem. Phys.* **2006**, *125*, 194101–1–17. (c) Zhao, Y.; Truhlar, D. G. *J. Phys. Chem. A* **2005**, *109*, 5656–5667.

(28) (a) Becke, A. D. *Phys. Rev. A* **1988**, *38*, 3098–3100. (b) Becke, A. D. *J. Chem. Phys.* **1993**, *98*, 5648–5652. (c) Lee, C.; Yang, W.; Parr, R. G. *Phys. Rev. B* **1988**, *37*, 785–789.

(29) Bharadwaj, P.; Novotny, L. *J. Phys. Chem. C* **2010**, *114*, 7444–7447.

(30) The value of 1.5 eV agrees well with the value deduced from the emission wavelength of $Sc_3N@C_{80}$ in ref 15a, whereas the emission of $La_2@C_{80}$ or **4** is too weak to be detected under our experimental conditions.

(31) Cook, S.; Furube, A.; Katoh, R.; Han, L. *Chem. Phys. Lett.* **2009**, *478*, 33–36.

(32) Yamamoto, K.; Saunders, M.; Khong, A.; Cross, R. J.; Grayson, M.; Gross, M. L.; Benedetto, A. F.; Weisman, R. B. *J. Am. Chem. Soc.* **1999**, *121*, 1591–1596.

(33) (a) Luo, C.; Guldi, D. M.; Imahori, H.; Tamaki, K.; Sakata, Y. *J. Am. Chem. Soc.* **2000**, *122*, 6535–6551. (b) Guldi, D. M.; Hirsch, A.; Scheloske, M.; Dietel, E.; Troisi, A.; Zerbetto, F.; Prato, M. *Chem.—Eur. J.* **2003**, *9*, 4968–4979. (c) Spänig, F.; Ruppert, M.; Dannhäuser, J.; Hirsch, A.; Guldi, D. M. *J. Am. Chem. Soc.* **2009**, *131*, 9378–9388.

(34) Tsuchiya, T.; Akasaka, T.; Nagase, S. *Bull. Chem. Soc. Jpn.* **2009**, *82*, 171–181.

(35) (a) The energy levels of the charge-separated states (ΔG_{RIP}) were evaluated using the Weller-type approach (see Supposting Information). (b) Rehm, D.; Weller, A. *Isr. J. Chem.* **1970**, *7*, 259–271.

(36) (a) Hay, P. J.; Wadt, W. R. *J. Chem. Phys.* **1985**, *82*, 299–310. (b) Binkley, J. S.; Pople, J. A.; Hehre, W. J. *J. Am. Chem. Soc.* **1980**, *102*, 939.